AIAA JOURNAL
Vol. 42, No. 2, February 2004

# Validation of Wilcox $k$–$\omega$ Model for Flows Characteristic to Hypersonic Airbreathing Propulsion

Bernard Parent*
*Seoul National University, Seoul 151-744, Republic of Korea*
and
Jean Pascal Sislian†
*University of Toronto, Downsview, Ontario M3H 5T6, Canada*

**Numerical results obtained with the WARP code solving the 1988 Wilcox $k$–$\omega$ two-equation model are compared with experimental data of flowfields characteristic of hypersonic airbreathing propulsion. The problems chosen for the comparison include a shock/boundary-layer interaction case, a reacting and inert planar mixing case, and two ramp injector mixing cases. In addition, a comparison is performed with empirical correlations on the basis of skin friction for flow over a flat plate and shear layer growth for a free shear layer. The agreement between the numerical and experimental results varies between being reasonable and excellent, with a discrepancy generally not exceeding 20%. It is found that the grid-induced error can be reduced to an acceptable level for most problems with a reasonable mesh size. However, the free shear layer and the shock/boundary-layer interaction cases require a considerably finer mesh. The Wilcox dilatational dissipation correction is seen to be beneficial in predicting the growth of a free shear layer at a high convective Mach number, but its use is considered either questionable or detrimental for the other cases. A proper choice of the turbulent Schmidt number is observed to be crucial in predicting the injectant mole fraction contours for one of the ramp injector cases, with the best agreement obtained with Schmidt number $Sc_t$ fixed to 0.25. For the inert planar mixing case, overall better agreement is obtained when setting both the turbulent Prandtl and Schmidt number to 0.5.**

## Nomenclature

| | | |
|---|---|---|
| $a$ | = | speed of sound |
| $C_f$ | = | skin-friction coefficient, $2\tau_w/\rho_\infty q_\infty^2$ |
| $C_\delta$ | = | problem-dependent parameter used in the Roshko–Dimotakis shear layer growth correlation |
| $c$ | = | species mass fraction |
| $i, j, k$ | = | grid coordinates |
| $J^{-1}$ | = | inverse of the metric Jacobian |
| $k$ | = | turbulence kinetic energy (TKE) |
| $k_{\text{div}}$ | = | user-specified constant used in conjunction with the present implementation of the $k$–$\omega$ model |
| $M$ | = | Mach number |
| $\mathcal{M}$ | = | molecular weight |
| $M_c$ | = | convective Mach number, $(q_1 - q_2)/(a_1 + a_2)$ |
| $M_t$ | = | turbulent Mach number, $\sqrt{(2k/a)}$ |
| $P$ | = | pressure |
| $P_k$ | = | production term of the TKE transport equation |
| $Pr$ | = | Prandtl number |
| $q$ | = | magnitude of the velocity vector |
| $Re$ | = | Reynolds number |
| $R_\Delta$ | = | discretized residual |
| $Sc$ | = | Schmidt number |
| $S_\omega$ | = | source term of the TKE specific dissipation rate equation |
| $T$ | = | temperature |
| $x, y, z$ | = | Cartesian coordinates |
| $\bar{x}, \bar{y}, \bar{z}$ | = | normalized Cartesian coordinates |
| $y^+$ | = | nondimensional wall distance, $y/\mu\sqrt{(\rho\tau_w)}$ |
| $\epsilon$ | = | dissipation rate of the TKE |
| $\mu$ | = | viscosity |
| $\xi$ | = | convergence criterion |
| $\xi_{\text{verge}}$ | = | user-defined convergence criterion threshold |
| $\rho$ | = | density |
| $\tau_w$ | = | wall shear stress |
| $\omega$ | = | dissipation rate per unit of TKE |

*Subscripts*

| | | |
|---|---|---|
| $k$ | = | $k$th species |
| $t$ | = | turbulent |
| $w$ | = | wall |
| 1 | = | first stream of a planar shear layer |
| 2 | = | second stream of a planar shear layer |
| $\infty$ | = | freestream |

Received 18 April 2003; revision received 24 September 2003; accepted for publication 8 October 2003. 

*Research Associate, Department of Aerospace Engineering; bernard@snu.ac.kr.

†Professor, Department of Aerospace Sciences and Engineering, Institute for Aerospace Studies; sislian@caius.utias.utoronto.ca. Associate Fellow AIAA.

## Introduction

ACCURATE prediction of the flowfields in and around the various components of hypersonic airbreathing vehicles through computational methods has become an area of increasing interest in recent years. This high interest in accurate computational results originates partly from the difficulty in obtaining in a laboratory environment the high flow speed and enthalpy characteristic of high-speed flight and partly from the difficulty in measuring all flow quantities and parameters of interest. One such parameter that needs to be assessed accurately is the skin friction along the body surface, which can account for a substantial portion of the total drag on the vehicle.[1] Of equal importance is the prediction of the inert or reacting mixing layer in either the inlet [1–3] or the combustor,[4–6] especially that originating from ramp injectors[7] and its variants.[8–10] Other flow regions that are also particularly difficult to predict numerically are shock/boundary-layer interactions. These can occur in the inlet and especially the combustor of the vehicle where strong shocks intersect a thick boundary layer. Recirculation regions associated with these interactions can significantly alter the skin friction and increase the heat load on the surface of the vehicle.

Hence, modern numerical methods need to be validated to available experimental data of the mentioned flows if confidence in them is to be gained in predicting the flow in and around hypervelocity airbreathing vehicles. Wilcox[11] used the Settles et al.[12] shock/boundary-layer interaction case, a variant of the Brown and Roshko,[13] Papamoschou and Roshko,[14] and Dimotakis[15] compressible shear layer growth correlation, and the Van Driest II skin-friction correlation to validate the Wilcox dilatational dissipation correction[11] when used in conjunction with the 1988 Wilcox $k$–$\omega$ model.[16] For some cases however, it is not clear what the magnitude of the grid-induced error is. In Ref. 17, Marshall and Kurkov investigate experimentally and numerically an inert mixing layer between hydrogen and vitiated air. Excellent agreement is obtained on the basis of the species mole fraction, and reasonable agreement is obtained on the basis of flow stagnation temperature, Mach number, and pitot pressure. A reacting mixing layer between hydrogen and a mixture of vitiated air and oxygen is also presented, for which the numerical method underestimates the reacting mixing layer growth by approximately 33%. The numerical method of Marshall and Kurkov uses an algebraic turbulence model, and there is no assessment of the grid-induced error. Waitz et al.[7] compare the helium mass fractions of a Mach 6 ramp injector flowfield obtained experimentally to the ones obtained using a laminar version of the SPARK[18,19] code. Partly because of the too coarse mesh in use and partly because of the absence of a turbulence model, the mixing rates are not captured accurately and the numerical results are used primarily to gain better physical insight in the mechanisms responsible for the formation of the axial vortices. Later, the experimental data of Waitz et al.[7] is used by Lee et al.[20] to validate numerical results obtained with the 1988 Wilcox[16] $k$–$\omega$ model including the Wilcox dilatational dissipation. Overall good agreement is observed on the basis of the maximum injectant mass fraction decay, but neither the impact of the dilatational dissipation correction nor the grid-induced error is quantified. In Ref. 8, Donohue et al. compare experimental data of a Mach 2 swept ramp injector flowfield to numerical results obtained with the SPARK code used in conjunction with the algebraic Baldwin–Lomax turbulence model without a compressibility correction. The authors[8] observe some unreasonably high values of the turbulent viscosity and suggest that a two-equation turbulence model might be better suited for this flowfield. It is not stated what the grid-induced error is.

In this paper, numerical results are compared with the already mentioned experimental data of Settles et al.,[12] Marshall and Kurkov,[17] Waitz et al.,[7] and Donohue et al.,[8] as well as with the Van Driest II skin-friction correlation and the Roshko–Dimotakis shear layer growth correlation (see Refs. 13 and 15). The numerical results are obtained with the WARP code[10,21] using a two-equation turbulence model coupled with a dilatational dissipation correction and the Jachimowsky[22] hydrogen–air chemical solver. Particular emphasis is given to quantifying the impact of the dilatational dissipation correction and the grid-induced error for all problems presented.

## Description of the Numerical Method

The numerical method solves the multispecies Favre-averaged Navier–Stokes equations closed by the 1988 Wilcox two-equation $k$–$\omega$ turbulence model[16] and the Wilcox dilatational dissipation.[11] Unless otherwise specified, the turbulent Schmidt number and the turbulent Prandtl number are fixed to 1.0 and 0.9, respectively. The freestream value of $\omega$ is set to $10q_\infty/\text{m}$. When applicable, the 9-species 22-reaction Jachimowski chemical model[22] is used. A structured mesh is used with the governing equations written in generalized coordinates following the approach by Viviand[23] and Vinokur.[24] Second-order-accurate discretization stencils are used for all derivatives, except for the convection derivative, which is discretized using the Yee–Roe flux-limited scheme (see Refs. 25 and 26). No entropy correction is used because it is unnecessary for the problems tackled herein and it increases significantly the grid-induced error.[10] High-temperature polynomials[27] are used to determine the enthalpy and the specific heat at constant pressure. The set of equations is iterated in pseudotime using a block-implicit approximate-factorization algorithm[28,29] and the marching window acceleration technique.[21] Convergence is attained when $\xi \le \xi_{\text{verge}}$ for all inner nodes part of the computational domain, with $\xi_{\text{verge}}$ a user-defined constant and $\xi$ defined as in Ref. 21, that is, as the maximum between the residual of the continuity and energy flux-conservation equations:

$$\xi \equiv \max\left(\frac{\sum_{k=1}^{n_s}\left|R_\Delta^{k\text{th continuity}}\right|}{J^{-1}\rho}, \frac{R_\Delta^{\text{energy}}}{J^{-1}\rho E}\right) \tag{1}$$

with the discretized residual $R_\Delta$ corresponding to the sum of all discretized derivatives. To enhance the robustness of the pseudotime integration, it was found necessary to modify the source term of the specific dissipation rate equation in the following manner[21]:

$$S_\omega = \frac{J^{-1}\omega}{\max[k, \min(k_{\text{div}}, \omega\mu/\rho)]}\left(\frac{5}{9}P_k - \frac{5}{6}\rho k\omega\right) \tag{2}$$

with $k_{\text{div}}$ a user-specified constant. For $k_{\text{div}} = 0$, the latter becomes the specific dissipation rate source term as outlined by Wilcox.[16] For $k_{\text{div}} > 0$, a higher pseudotime step can be used, improving the convergence rate. The minimum between $k_{\text{div}}$ and $\omega\mu/\rho$ is taken so that the specific dissipation rate equation is modified only in nonturbulent flow regions, such as the laminar subregion of the turbulent boundary layer, for example. In addition to permitting larger pseudotime steps to be used, the latter modification is here necessary to prevent a division by zero in the source term of the $\omega$ transport equation because the turbulence kinetic energy sometimes decreases to negative values when hydrogen–air mixing problems are solved. This is attributed to the lack of positivity preservation of the Yee–Roe scheme, which is here used to solve in coupled form the convection terms of all transport equations. It is essential to apply the Yee–Roe scheme to all transport equations to retain the monotonicity preservation property of the Roe scheme due to the strong coupling between the $k$ transport equation and the fluid flow equations (see Ref. 21).

Note that the user-defined parameters $\xi_{\text{verge}}$ and $k_{\text{div}}$ can affect the results substantially when set to a too high value. For this reason, particular care is taken for all cases shown herein in ensuring that the error originating from $\xi_{\text{verge}}$ and $k_{\text{div}}$ is minimized and remains significantly below the grid-induced error.

## Comparison with Empirical Correlations

### Flat Plate

In contrast to the $k$–$\epsilon$ models, a property of the $k$–$\omega$ model is its inherent ability to solve the laminar subregion of the turbulent boundary layer without the introduction of additional low Reynolds number terms or the use of wall functions. This is particularly important in the accurate prediction of shock/boundary-layer interaction problems and other problems where the boundary layer is subject to an adverse pressure gradient.[30] However, the addition of the Sarkar (see Ref. 31) dilatational dissipation terms affects the accuracy of the baseline model as the freestream Mach number increases; this is observed in the simulation of an adiabatic flat plate at a freestream Reynolds number per meter of $5 \times 10^6$, at a temperature of 120 K and at a Mach number varied between 0.3 and 6. (The problem setup is shown in Fig. 1.) The shear stress is measured at the outflow, 1 m downstream of the leading edge. A $392 \times 300$ grid with the first node distant from the wall by 5, 5, 10, and 15 $\mu$m for the freestream

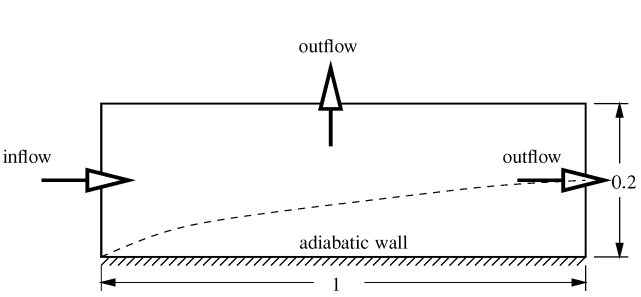


**Fig. 1 Schematic of the flowfield, computational domain, and boundary conditions for the flat plate validation case; all dimensions in meters.**

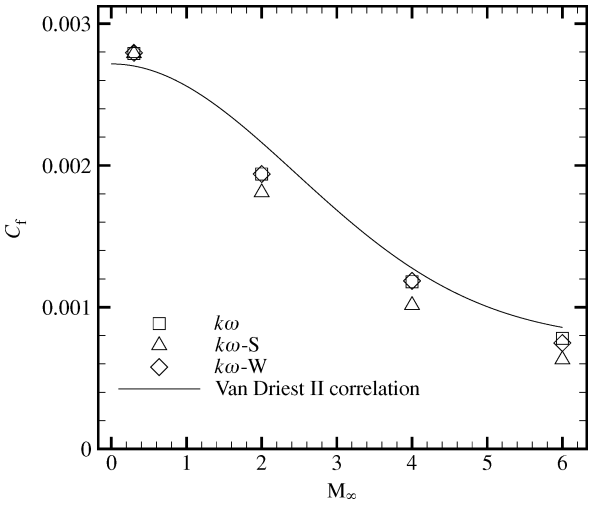


**Fig. 2 Skin-friction coefficient at the trailing edge of an adiabatic flat plate vs freestream Mach number; $T_\infty = 120$ K, $Re_\infty = 5 \times 10^6$/m with air the medium; $k$–$\omega$, $k$–$\omega$-S, and $k$–$\omega$-W refer to the $k$–$\omega$ model used with no dilatational dissipation correction, with the Sarkar dilatational dissipation correction, and with the Wilcox dilatational dissipation correction, respectively.**

Mach number 0.3, 2, 4 and 6, respectively. For each case, this is found to result in a value of the nondimensional wall distance $y^+$ smaller than unity for most of the length of the flat plate. The user-defined parameter $\xi_{\text{verge}}$ is here set to 50/s for a freestream Mach number of 2, 4, and 6 and to 1/s for a freestream Mach number of 0.3.

For a freestream Mach number of 4, an estimate of the error on the skin-friction coefficient is performed by solving four different grids, that is, $98 \times 75$, $196 \times 150$, $392 \times 300$, and $784 \times 600$. For the baseline $k$–$\omega$ model, the skin-friction coefficient 1 m downstream from the leading edge is seen to correspond to 0.00131, 0.00122, 0.001181, and 0.001167. The $392 \times 300$ mesh overestimates the skin-friction coefficient by approximately 2% and is the mesh size used to obtain the data shown in Fig. 2. Figure 2 shows a comparison of the skin-friction coefficient obtained numerically to the Van Driest II correlation. Note that, due to the low freestream temperature, high-temperature effects are negligible, and a calorically perfect gas can be assumed. This is important when comparing with the Van Driest II correlation because the latter does not take into account high-temperature effects of the gas. At least up to Mach 6, the Wilcox modeling of the dilatational dissipation term (denoted by $k$–$\omega$-W) does not significantly alter the shear stress, whereas the Sarkar modeling (referred to by $k$–$\omega$-S) causes a decrease in $C_f$ of 19% at the highest freestream Mach number. Although it exhibits good performance, the Wilcox correction is tested here only for a flow Mach number not exceeding 6 due to lack of reliable experimental data for higher Mach numbers. Whether the Wilcox dilatational dissipation correction remains accurate at a freestream Mach number in excess of 6 is questionable.

For a freestream Mach number of 0.3, 2, 4, and 6, it is found that the maximum value of $k$ in the boundary layer at the domain exit is approximately 16, 850, 4000, and 10,000 $\text{m}^2/\text{s}^2$, respectively. At a freestream Mach number of 2, a $k_{\text{div}}$ value of 1, 100, and 800 $\text{m}^2/\text{s}^2$ is found to translate to a skin-friction coefficient at the domain exit of $2.00 \times 10^{-3}$, $1.96 \times 10^{-3}$, and $1.41 \times 10^{-3}$ units, respectively. Hence the thickness of the boundary layer at the exit is seen to be decreased by 21% when $k_{\text{div}}$ is set to 800 $\text{m}^2/\text{s}^2$ and decreased by 2% when $k_{\text{div}}$ is set to 100 $\text{m}^2/\text{s}^2$. Therefore, a value given to $k_{\text{div}}$ less than 1/10th of the maximum value of $k$ in the boundary layer results in a shear stress and boundary-layer thickness within 2% of the value obtained with a vanishing $k_{\text{div}}$. Hence, we set $k_{\text{div}}$ to 100 $\text{m}^2/\text{s}^2$ for the freestream Mach numbers 2, 4, and 6. Interestingly, for a freestream Mach number of 0.3, a value of $k_{\text{div}}$ approximately 10 times less than the maximum value of $k$ in the boundary-layer profile, that is, 2 $\text{m}^2/\text{s}^2$, is found not to be sufficiently small and translates in a 7% overestimation in the shear stress and in a 13% overestimation in the boundary-layer height at the domain exit. A value for $k_{\text{div}}$ of 0.001 $\text{m}^2/\text{s}^2$ is hereafter chosen for this freestream Mach number. The sensitivity of the $k$–$\omega$ model to the user-specified parameter $k_{\text{div}}$ is seen to be more important for subsonic boundary layers than for supersonic ones; for subsonic boundary layers, it is suggested to use a value for $k_{\text{div}}$ smaller than 1/100th the maximum value of $k$ in the boundary-layer profile. For supersonic flows, using a $k_{\text{div}}$ value 1/10th the maximum value of $k$ in the boundary-layer profile is sufficient for a 2% accuracy on the wall shear stress and boundary-layer thickness.

### Compressible Shear Layer

Despite its apparent simplicity, a turbulent shear layer is one of the most difficult turbulent flowfields to solve using a two-equation model.[30] In addition, shear layers obtained experimentally[14] with convective Mach numbers in excess of 0.5 exhibit a reduction in growth rate with increasing $M_c$, which requires the addition of a dilatational dissipation term to the turbulence model. As shown in Fig. 3, a 2-m-long shear layer is investigated herein and compared to the empirical correlation proposed by Brown and Roshko[13] and Brown[32] multiplied by the compressibility correction factor for compressible shear layers outlined by Papamoschou and Roshko[14] and later by Dimotakis.[15] This empirical correlation is here referred to as the Roshko–Dimotakis correlation and can be written as

$$\text{growth}_{\text{Roshko-Dimotakis}} = \frac{1}{2} C_\delta \times \underbrace{(q_1 - q_2)}_{\substack{\text{speed difference} \\ \text{between the two} \\ \text{streams}}} \times \underbrace{\frac{\sqrt{\rho_1} + \sqrt{\rho_2}}{q_1\sqrt{\rho_1} + q_2\sqrt{\rho_2}}}_{\substack{\text{inverse of} \\ \text{incompressible} \\ \text{average speed}}} \times \underbrace{\frac{1 + 4\exp\left(-3M_c^2\right)}{5}}_{\substack{\text{Papamoschou-Roshko} \\ \text{correction for} \\ \text{compressible shear layer}}} \tag{3}$$

where $C_\delta$ is a problem-dependent parameter that usually lies between 0.25 and 0.45. Note that the incompressible average speed (outlined in the latter equation) is found by equating the incompressible stagnation pressure of both streams in a Galilean frame of reference traveling at a speed equal to the incompressible convective velocity with respect to the laboratory frame of reference (see Dimotakis[15]). For simplicity, the effect of a density difference[13] on the shear layer growth is not included in Eq. (3) because this effect tends to be very small. (It alters the growth by less than 5% for even the highest density difference tested experimentally.) Figure 4 shows the magnitude of the Papamoschou–Roshko compressibility correction for a convective Mach number range $0 < M_c < 2.4$. Equation (3) shows that the shear layer growth is proportional to the difference in speed between the two streams and inversely proportional to the incompressible average speed, which always lies between the speed of both streams. This is an important property of

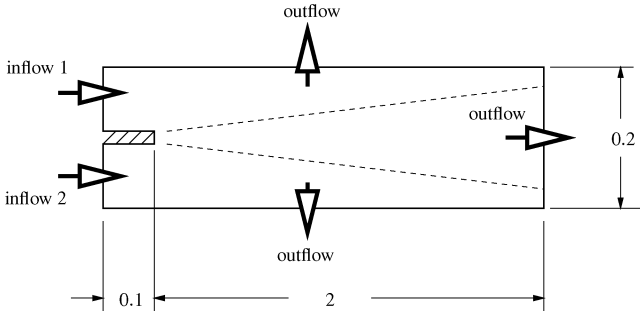


**Fig. 3 Schematic of the computational domain setup for the shear layer validation cases; all dimensions in meters.**

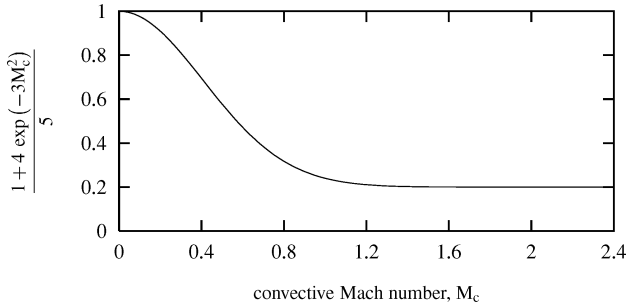


**Fig. 4 Empirically based shear layer growth correction factor by Papamoschou and Roshko[14] vs the convective Mach number.**

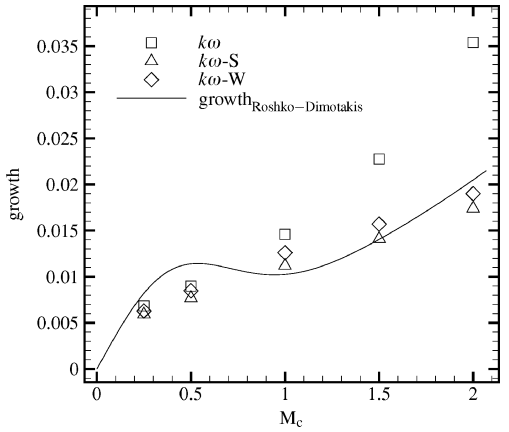


**Fig. 5 Shear layer growth between Mach 7 and Mach $7-2M_c$ airstreams; $P=10$ kPa and $T=300$ K for both jets; to determine the Roshko–Dimotakis shear layer growth, $C_\delta$ fixed to 0.25.**

the shear layer growth, which explains the reduced mixing occurring for a high Mach number and high temperature flow compared to a flow with high Mach number but low temperature.

Before the shear layer start, a short 10-cm-long flat plate is applied to the two jets to prevent a singularity at the point of injection. Air is the medium for both streams at a pressure of 10 kPa and a temperature of 300 K. The inflow Mach number of the second stream is fixed to 7, while the inflow Mach number of the first stream is set to $7-2M_c$. The convective Mach number of the system can be taken as $M_c=(q_1-q_2)/(a_1+a_2)$ with $q$ the speed and $a$ the sound speed and the subscripts 1 and 2 referring to each of the two jets at the inflow section. The user-defined parameters $k_{\text{div}}$ and $\xi_{\text{verge}}$ are set to 1.1 $\text{m}^2/\text{s}^2$ and 10/s.

To assess the error originating from the grid, three mesh levels are computed and the solution compared. At a convective Mach number of 1.0, using the Wilcox dilatational dissipation correction and grid size of $191\times80$, $381\times160$, and $762\times320$ nodes is observed to result in a shear layer growth (measured as the height of the shear layer at $x=2.0$ m divided by 2 m) of 0.0150, 0.0134, and 0.0126, respectively. A $762\times320$ mesh is chosen to perform all simulations shown in Fig. 5, with the grid-induced error for that mesh size estimated to translate to a 6% overestimation of the shear layer growth. Note that the mesh is constructed such that the gridlines are aligned with the $x$-velocity contours and that 75% of the grid points along the cross-stream grid coordinate $j$ are ensured to be inside the shear layer at any $x$ station for the $M_c=1$ case. The same mesh is used for all cases. The shear layer growth for $0<M_c<2$ is shown in Fig. 5. Both the Wilcox and Sarkar modeling of the dilatational dissipation term improve the baseline $k$–$\omega$ model, and the agreement with the empirical correlation is good for $C_\delta$ here fixed to 0.25.

## Comparison with Experimental Data

### Settles et al.[12] Shockwave/Turbulent Boundary-Layer Interaction

Experimental data of a shock/boundary-layer interaction problem that is widely used in the computational fluid dynamics (CFD) community to validate turbulence models and/or compressible CFD methods is the Mach 2.84 wedge flow by Settles et al.[12] (schematized in Fig. 6). The incoming air stagnation temperature is of 262 K, which results in a freestream temperature of 98 K. The freestream Reynolds number per meter is set to $6.3\times10^7$, whereas the inflow Mach number is set to 2.84. Through a trial-and-error approach, a flat plate length of 2.2 m is here found adequate in generating a 2.11-cm boundary-layer thickness at the start of the separation bubble, in accordance with experimentally observed results. No entropy correction is used in conjunction with the Yee–Roe scheme. Values of 7/s and 1 $\text{m}^2/\text{s}^2$ are used for $\xi_{\text{verge}}$ and $k_{\text{div}}$, respectively. Because of the relatively high freestream Reynolds number, a small wall node spacing of 1 $\mu$m is necessary to ensure a value of $y^+$ below 1 for most of the flat plate and wedge. Note that the use of a small wall node spacing is found to be particularly important when measuring the skin-friction coefficient $C_f$, but less important in measuring the pressure at the wall. The mesh is designed such that approximately 25% of the grid lines in the streamwise direction and 70% of the gridlines in the cross-stream direction are allocated to the recirculation bubble. A grid-convergence study of the skin-friction coefficient and wall pressure is shown in Fig. 7. The comparison between the latter properties is performed using grids consisting of $220\times110$ nodes, $440\times220$ nodes, and $880\times440$ nodes. It is found

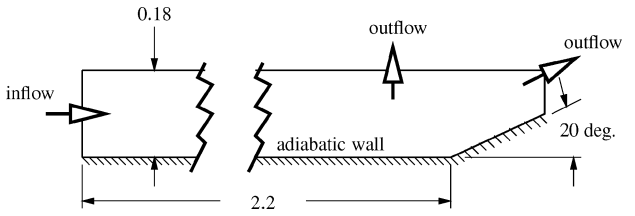


**Fig. 6 Grid design of the Settles et al.[12] shockwave/turbulent boundary-layer interaction problem; all dimensions in meters unless otherwise noted.**

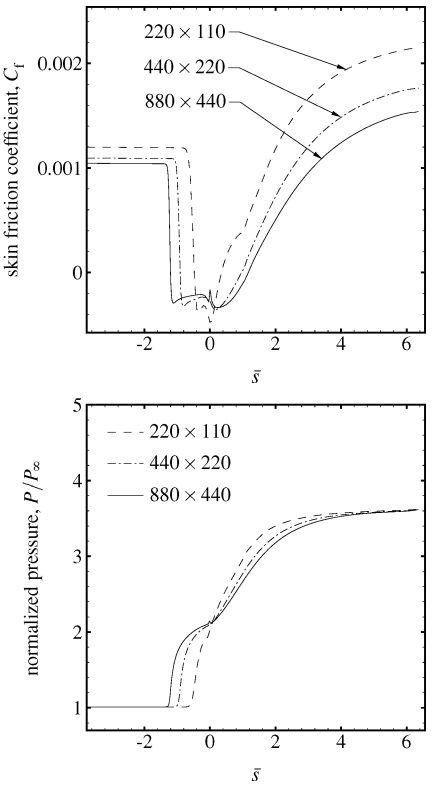


**Fig. 7 Grid convergence study of the skin-friction coefficient and the normalized pressure along the wall for the Settles et al.[12] case using the Wilcox $k$–$\omega$ model including the Wilcox dilatational dissipation correction; $\bar{s}$ is the distance along the wall normalized with the boundary-layer height (2.11 cm).**

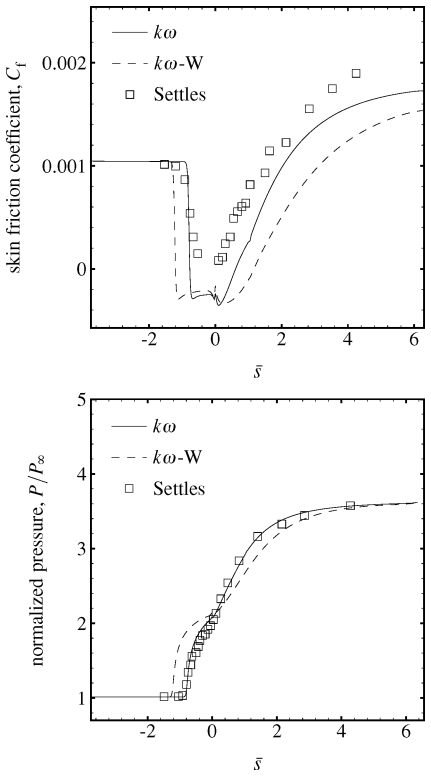


**Fig. 8 Skin-friction coefficient and normalized pressure along the wall for a wedge angle of 20 deg; grid size of 880 × 440 nodes used; $\bar{s}$ is the distance along the wall normalized with the boundary layer height (2.11 cm).**

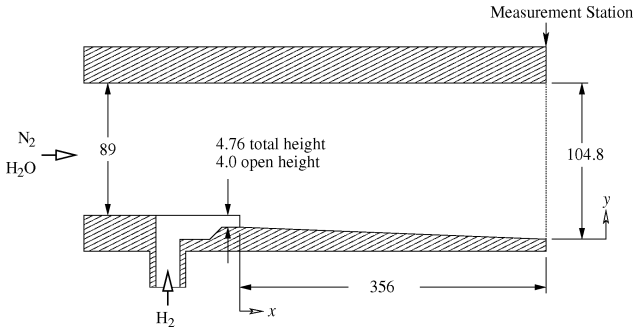


**Fig. 9 Experimental setup of the Marshall–Kurkov planar mixing problem[17]; all dimensions in millimeters.**

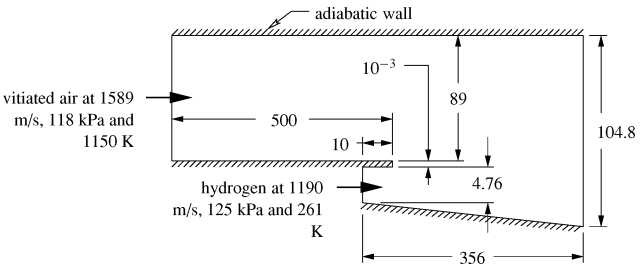


**Fig. 10 Boundary conditions and computational domain dimensions (in millimeters) used to reproduce the Marshall–Kurkov mixing problem.[17]**

that even for the finest mesh, the solution still exhibits a somewhat significant dependency on the grid. When it is assumed that the trend shown would remain as the mesh is further refined, it is estimated that, for the finest mesh, the error on the skin-friction coefficient is of 5% before the recirculation bubble and of 15% along the compression surface. The error of the pressure is estimated to be of 4% on the compression surface. The error of the size of the recirculation bubble along the streamwise coordinate is estimated to be of 20%. Because of the high number of effective iterations needed for convergence (1294, 2186, and 4768 effective iterations for the coarse, medium, and fine meshes, respectively), a solution on an even finer mesh proved to be too time consuming with current computational capabilities.

With use of a mesh of $880 \times 440$ nodes, a comparison is made in Fig. 8 between the baseline $k$–$\omega$ model and the baseline $k$–$\omega$ with the Wilcox dilatational dissipation correction ($k$–$\omega$-W). The Sarkar modification is not presented here because it is not applicable to wall bounded flows. Interestingly, better agreement with experimental data is obtained using the baseline $k$–$\omega$ model, without the inclusion of the dilatational dissipation term. Note that Settles et al.[12] observed the length of the separation as obtained by oil flow measurements to be significantly larger than the one obtained from the surface pressure. It is argued by the experimentalists that the shock is not perfectly steady and exhibits a low-frequency oscillation in the streamwise direction. This is postulated to be the cause of the discrepancy observed experimentally between the size of the separation bubble deduced from the skin friction and the pressure measurements. It is possible that, without this oscillation, the experimental pressure measurements would indicate a somewhat larger separation bubble, resulting in a better performance of the dilatational dissipation correction.

### Marshall–Kurkov[17] Planar Mixing Problem

A numerical and experimental investigation of a planar mixing layer problem between vitiated air and hydrogen was performed by Marshall and Kurkov.[17] The experimental apparatus setup is shown schematically in Fig. 9. The vitiated air corresponds to a mixture of water vapor and nitrogen in mass proportions of 0.768:0.232. The computational domain dimensions and boundary conditions used to reproduce numerically the experiment setup are shown in Fig. 10. The user-adjustable parameters $k_{\text{div}}$ and $\xi_{\text{verge}}$ are set to $100\ \text{m}^2/\text{s}^2$ and 100/s, respectively, and no entropy correction term is used in conjunction with the Yee–Roe scheme. A 4.76-mm hydrogen step height is used, and the thickness of the wall separating the hydrogen jet from the incoming air is assumed negligible and set to zero. A 50-cm-long flat plate is found necessary to create the 1-cm-thick incoming boundary layer at $x = 0$ present in the experiments. Note that the thickness of the incoming air boundary layer plays a small role in the mixing process and is not considered critical to the success of this simulation. The hydrogen jet inflow velocity is set to 1190 m/s, with a pressure of 125 kPa and a temperature of 261 K. The air properties at $x = -0.5$ m are set to a velocity of 1589 m/s, a static pressure of 118 kPa, and a temperature of 1150 K. The wall boundary condition is adiabatic. Because of the flow Mach number being considerably less than 6, compressibility effects in the turbulent boundary layer are not present (Morkovin's hypothesis). In as much as the shear layer strength is also relatively small at a convective Mach number of ~0.21, no compressibility effect is expected in the mixing layer as well. This is confirmed by our numerical results: There is no discernible difference between the results obtained with the $k$–$\omega$ model (without the dilatational dissipation correction) and those obtained with the $k$–$\omega$-W model (with the Wilcox dilatational dissipation correction).

The entire flowfield is resolved using a $520 \times 380$ mesh, with 41% of the nodes allocated to the mixing region. The grid spacing at the wall is set to 1 $\mu$m, which results in a value of $y^+$ smaller than 1 for most of the flowfield, except in the vicinity of the hydrogen and air inflow boundaries. A comparison of results obtained using a $260 \times 190$, $520 \times 380$, and $1040 \times 760$ mesh reveals no significant difference between the volume fraction profiles, with the largest grid-induced error observed being in the stagnation pressure at the edge of the shear layer. The sharp turbulent/nonturbulent interface at the edge of the shear layer makes the stagnation pressure particularly sensitive to the grid, as can be seen in Fig. 11.

Qualitative good agreement is obtained between the $k$–$\omega$-W model and the Marshall–Kurkov[17] data, with a relative difference generally not in excess of 20%, on the basis of the volume fraction,

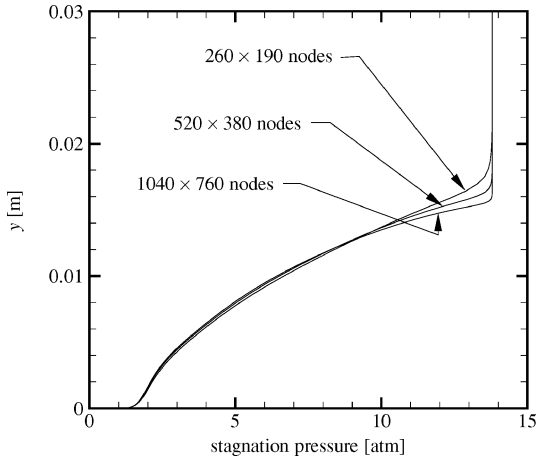


**Fig. 11 Grid convergence study between three mesh levels of the stagnation pressure measured at $x = 35.6$ cm; Wilcox dilatational correction is used alongside Wilcox $k$–$\omega$ model.**

pitot pressure, Mach number, and stagnation temperature, shown in Fig. 12. For all flow properties presented here, the best agreement between the $k$–$\omega$ model and the experimental results is obtained when the turbulent Schmidt number and turbulent Prandtl number are both set to 0.5. This is not surprising because the turbulent Prandtl number is recommended to be set to 0.5 when simulating shear layers (see Ref. 30). It is generally set to 0.9 to model correctly the temperature profiles in the turbulent boundary layer, which results in a better prediction of the heat flux at the wall. The largest discrepancy observed is in the flow stagnation temperature, with a relative difference of 40% between the computed and experimental data. This is believed to be an error in the experimental data rather than in the computed data because the experimental stagnation temperature profile indicates a larger mixing layer growth than the pitot pressure and Mach number profiles determined empirically.

In the preceding setup, note that the volume fraction corresponds to

$$\text{volume fraction of } k\text{th species} = \frac{c_k}{\mathcal{M}_k} \Bigg/ \sum_{l=1}^{n_s} \left( \frac{c_l}{\mathcal{M}_l} \right) \qquad (4)$$

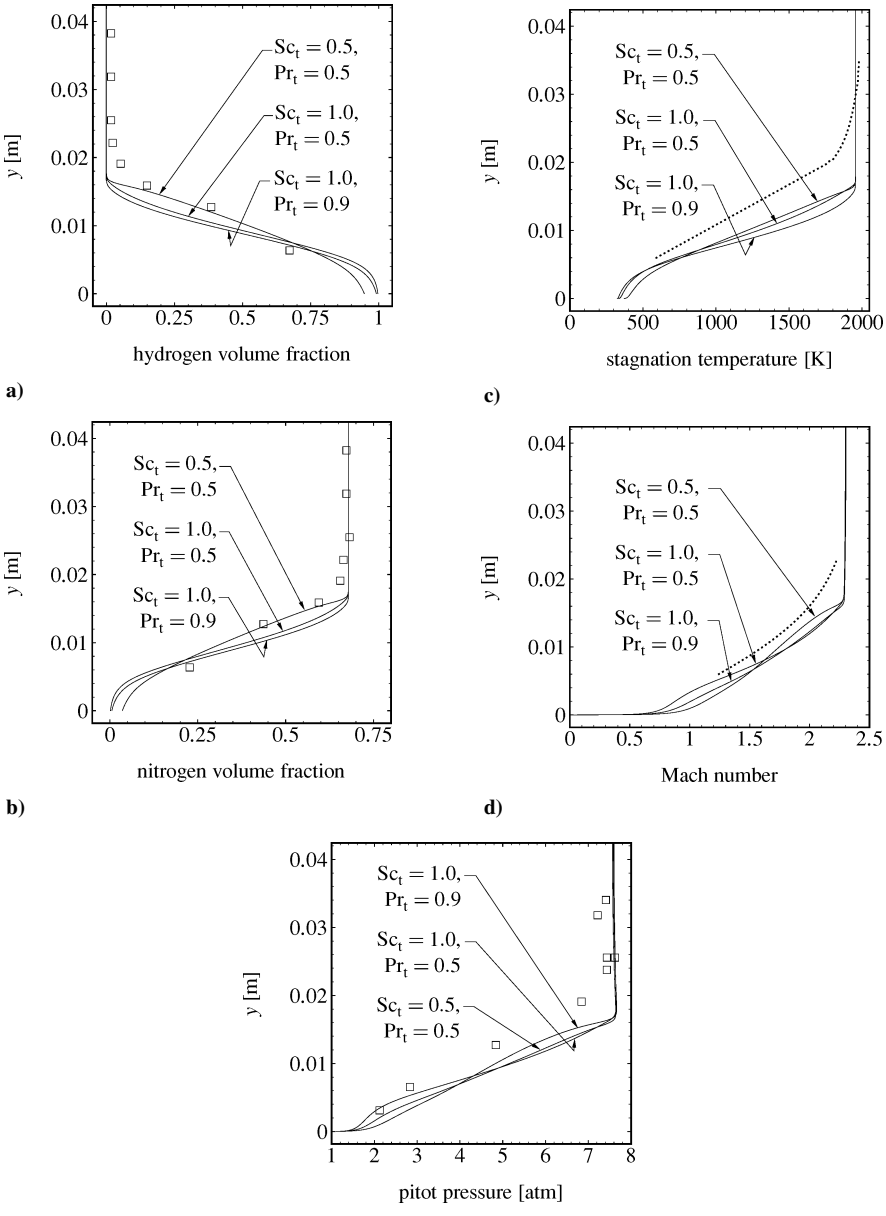


**Fig. 12 Comparison between numerical results and experimental data from Marshall and Kurkov[17] at $x = 35.6$ cm; numerical results obtained using mesh size of 520 × 380 nodes, using Wilcox dilatational dissipation correction alongside the Wilcox $k$–$\omega$ model.**

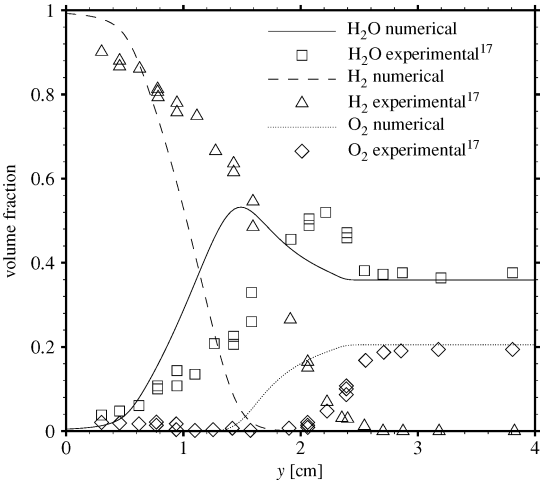


**Fig. 13 Species volume fraction at $x = 35.6$ cm for the reacting mixing layer case of Marshall and Kurkov.[17]**

whereas the stagnation pressure is obtained numerically, following the approach outlined in Ref. 33, and the stagnation temperature is determined from conservation of total enthalpy. In regions of subsonic flow, the pitot pressure is set to the stagnation pressure, and in regions of supersonic flow, the pitot pressure is set to the multiplication of the stagnation pressure by the stagnation pressure ratio found from the normal shockwave relation (which assumes a calorically perfect gas).

Using the same geometry as shown in Fig. 9, Marshall and Kurkov[17] further investigate a reacting mixing layer between hydrogen and a mixture of vitiated air and oxygen. Compared to the inert case, the inflow conditions for the hydrogen are not altered, whereas the inflow conditions for the vitiated air are changed to a temperature of 1260 K and a species composition of oxygen, water vapor, and nitrogen with the mass fractions being 0.26, 0.256, and 0.484, respectively. Neither the grid nor the air inflow speed and pressure are altered from the inert case. The nine-species ($H_2$, $O_2$, H, O, OH, $H_2O$, $HO_2$, $H_2O_2$, and $N_2$) Jachimowsky[22] chemical model is used along with WARP. Both the turbulent Prandtl number and Schmidt number are set to 0.5. The Wilcox dilatational dissipation is used in conjunction with the $k$–$\omega$ model. The comparison between our numerical results and the experimental data is shown in Fig. 13. The numerically obtained mixing layer growth underestimates that obtained experimentally by approximately 21% on the basis of the $y$ position of maximum water vapor volume fraction and by approximately 33% on the basis of the hydrogen volume fraction at the mixing layer edge. Marshall and Kurkov[17] observed a similar discrepancy on comparison with a space-marching method using an algebraic turbulence model.

### Waitz et al.[7] Ramp Injector

A Mach 6 ramp injector is investigated experimentally by Waitz et al.[7] with a geometry shown in Fig. 14. A 400-mm-long flat plate is here found necessary to create the experimentally observed boundary layer height of 5 mm at the injector start. Air enters the domain at a speed of 958 m/s, a pressure of 4370 Pa, and a temperature of 63.4 K. Helium is injected at an angle of 4.76 deg with respect to the $x$ axis, a speed of 1274 m/s, a pressure of 4370 Pa, and a temperature of 162.2 K. Note that, in the experiments, not all of the helium is injected at an angle of 4.76 deg. Rather, the angle of injection is noted by the experimentalists to be 0 deg near the bottom of the ramp and 4.76 deg at the top of the ramp. Because it is unclear how the angle of injection varies with the $y$ coordinate, we prefer to fix it everywhere to 4.76 deg. Although this is not expected to alter significantly the mixing rate, this could have an impact on the injectant mass flux center. The inflow velocities and temperatures result in a Mach number of 6.0 for the airstream, 1.7 for the helium jet, and a convective Mach number of 0.38. The user-defined parameters $k_{\text{div}}$ is set to 1000 $\text{m}^2/\text{s}^2$, which is 1/10th or less of the maximum value

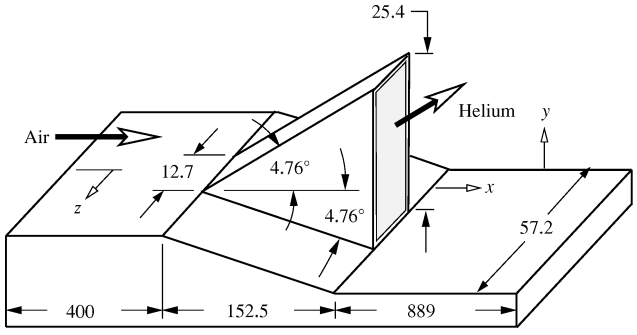


**Fig. 14 Schematic of Waitz et al.[7] ramp injector; all dimensions in millimeters unless otherwise specified.**

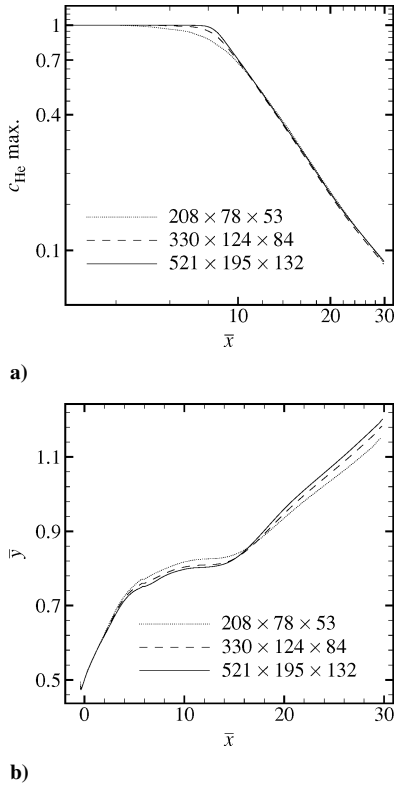


**Fig. 15 Grid convergence study for Waitz et al.[7] ramp injector case using Wilcox $k$–$\omega$ turbulence model without the dilatational dissipation; distances normalized with injector height 25.4 mm based on a) the maximum helium mass fraction of helium and b) the helium mass flux center.**

of $k$ in the incoming boundary layer and on the external surfaces of the injector. The convergence threshold $\xi_{\text{verge}}$ is set to 400/s, and the wall node spacing is fixed to 10 $\mu$m, which results in a value of $y^+$ at the wall of approximately 3 in the mixing region and along the flat plate upstream of the injector. Note that, although a somewhat lower value for $y^+$ is generally recommended along with the $k$–$\omega$ model, setting $y^+$ to 3 is here found to result in a minimal error of the boundary-layer thickness and wall shear stress. A lower value for $y^+$ would be detrimental for this problem because more grid lines would be needed near the surfaces, which would result in fewer grid lines allocated to the mixing layer. A grid-convergence study with meshes using $208 \times 78 \times 53$, $330 \times 124 \times 84$, and $521 \times 195 \times 132$ grid points reveals a negligible numerical error at all mesh levels (Fig. 15) for the maximum helium mass fraction and the helium mass flux center. The medium mesh ($330 \times 124 \times 84$ nodes) is used to obtain the helium mass fraction decay and helium mass flux center shown in Figs. 16a and 16b. Good agreement with experimental data is reproduced, and the "goodness" of the mixing is striking: In a mixing region length less than 1 m, the maximum helium mass

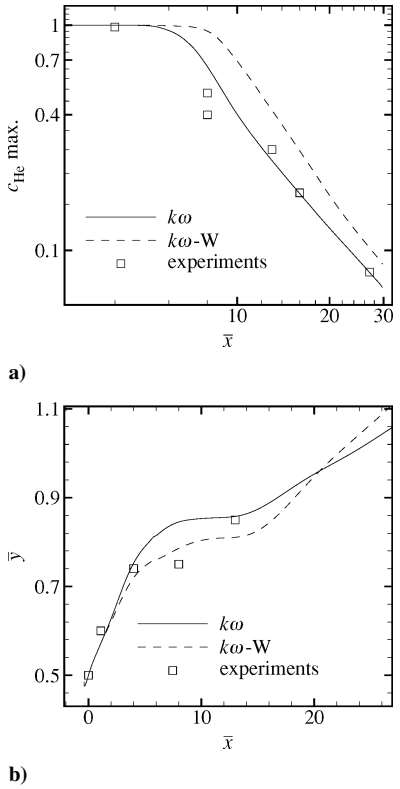


**Fig. 16 Comparison between $k$–$\omega$/$k$–$\omega$-W models and the Waitz et al.[7] ramp injector experimental data with grid of 330 × 124 × 84 nodes and distances normalized with the injector height 25.4 mm, based on a) the maximum helium mass fraction of helium and b) the helium mass flux center.**

fraction drops below 0.1. Although this flowfield is hypersonic, and hypersonic flowfields are notorious for their very slow mixing, one should consider the very low freestream temperature that results in a very low flow speed (958 m/s). Because the growth of the shear layer is inversely proportional to the flow speed [Eq. (3)], it can be stated that, due to the very low freestream temperature, the Waitz et al.[7] ramp injector results in an optimistic prediction of the mixing layer growth (and, hence, the rate of decay of the maximum injectant mass fraction) as compared to a mixing scenario that would occur in nominal flight conditions. Furthermore, as can be observed in Fig. 16, the dilatational dissipation plays a small role, both in the boundary layer and in the mixing layer due to low convective Mach number and axial vortices strength. However, note that slightly better agreement is observed on the basis of the maximum injectant mass fraction when not using the dilatational dissipation correction. Last, although not shown here, the mixing is found to be reduced significantly when the flat plate length upstream of the injector is reduced from 400 to 0 mm (Fig. 14). This is believed to be due to an increased amount of turbulence convected from the boundary layer to the mixing layer, hence, augmenting the spreading rate of the mixing layer.

### Donohue et al.[8] Swept Ramp Injector

A Mach 2 swept ramp injector mixing problem is studied experimentally and numerically by Donohue et al.[8] Because of the advanced measuring technique utilized, the experimental results include the contours of many flow properties of interest at different cross-stream planes and serve as an excellent testbed for validating our numerical method. In this paper, however, only a comparison of the injectant mole fraction contours at different streamwise stations is shown. Mixing takes place in a 30-mm-deep and 18.1-mm-high duct using the swept injector design shown in Fig. 17. A grid composed of 2.4 million nodes is judged sufficient for this problem because it gives mass fraction contours of the injectant close to those obtained using a 0.33-million-node mesh. When the maximum volume fraction of the injectant at the domain exit obtained on the coarse mesh is compared to the one obtained on the fine mesh, a relative increase of only 18% is observed. To simulate the 2-mm-high incoming boundary layer present in the experiments, a 7-cm constant area duct is concatenated to the injector domain. A rectangular injectant jet (as opposed to a circular jet) is used in the numerical simulations to simplify the gridding process. The duct walls at $y = \pm 15.2$ mm are simulated as symmetry planes to concentrate the nodes in the mixing region. The wall node spacing is set to 6 $\mu$m, which translates into a value of $y^+$ of approximately 4 throughout the mixing region. The incoming air is set to a pressure of 30.8 kPa, a temperature of 163 K, and a Mach number of 2, whereas the injectant inflow is fixed to a speed of 470 m/s, a temperature of 180 K, and a mass flux of 0.00261 kg/s. Particular attention is given to matching the injectant speed and mass flow rate between the experiments and numerical simulation because these two parameters are known to influence the mixing process significantly.[10] Also, a short constant area runway of 2 mm is imposed to the injectant before injection. The user-adjustable parameters $k_{\text{div}}$ and $\xi_{\text{verge}}$ are set to 1100 $\text{m}^2/\text{s}^2$ and 300/s, respectively, and no entropy correction term is used along with the Yee–Roe scheme. The maximum value for the turbulence kinetic energy in the boundary layer is seen to vary between 1500 and 2500 $\text{m}^2/\text{s}^2$. Note that the value given to $k_{\text{div}}$

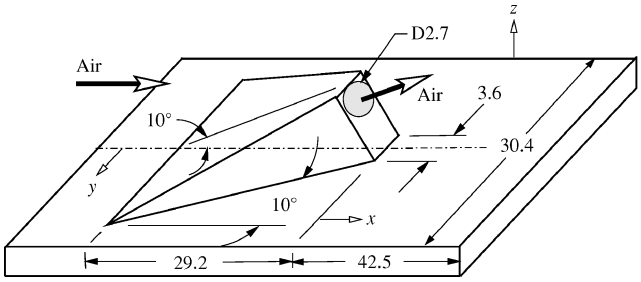


**Fig. 17 Schematic of Donohue et al.[8] swept ramp injector; all dimensions in millimeters unless otherwise specified.**

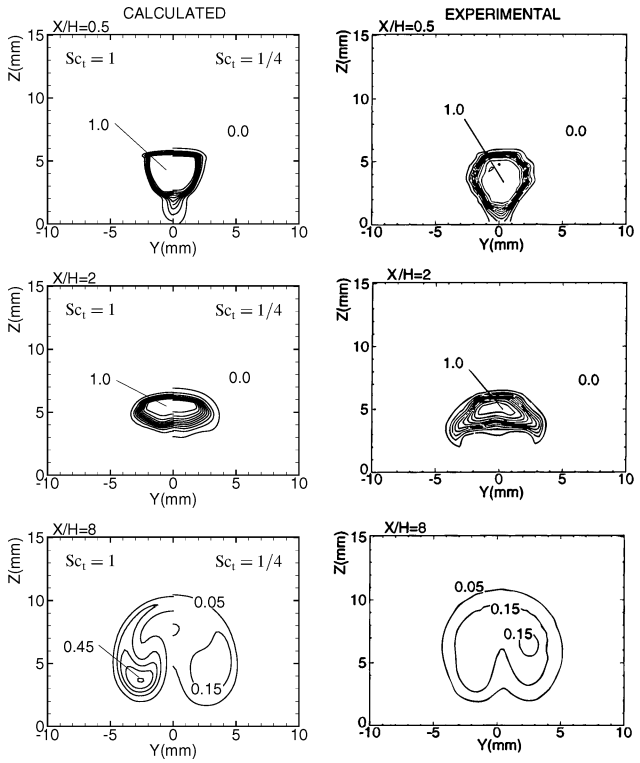


**Fig. 18 Injectant mole fraction at different $x$-stations for the Donohue et al.[8] injector case where $H$ is height of the injector, 5 mm. Experimental data reprinted with permission from AIAA.**

is not the recommended value of 1/10th the maximum value of $k$ in the boundary layer. However, it was not possible to obtain convergence at a lower value of $k_{\text{div}}$ in this case. Based on previous results for turbulent flat plates, a value of $k_{\text{div}}$ half the maximum value of $k$ in the boundary layer induces an error on the boundary-layer thickness of approximately 10%. This is considered acceptable for this problem because the injectant mole fraction is not expected to be significantly altered by small changes in the boundary-layer height. The dilatational dissipation correction is observed to play a small role in this case. An additional simulation ran without the dilatational dissipation showed a relative decrease of only 15% in the maximum injectant mole fraction at $x = 40$ mm. Figure 18 shows a comparison between the injectant mole fraction contours obtained experimentally and with the present numerical method on the planes $x = 2.5$, 10, and 40 mm. At a turbulent Schmidt number of 0.25, good agreement is shown on the basis of the shape and size of the region spanned by the injectant, and acceptable agreement is shown on the basis of the injectant mole fraction quantities. However, fixing Schmidt number $Sc_t$ to 1 results in underpredicted mixing and a maximum injectant mole fraction more than two times the one measured experimentally in far field (Fig. 18). Hence, a good choice of the turbulent Schmidt number is seen to be critical in the correct prediction of this flowfield.

## Conclusions

The agreement between our numerical results and the empirical correlations or experimental data presented herein varies between being reasonable and excellent. The largest discrepancies observed are of 40% on the basis of the flow stagnation temperature for the Marshall and Kurkov inert planar mixing case and of 33% on the basis of the mixing layer growth for the Marshall and Kurkov reacting mixing case. A discrepancy not exceeding 20% is observed on the basis of 1) the separation bubble streamwise length for the Settles et al. case, 2) the shear layer growth of two airstreams in the convective Mach number range $0 \leq M_c \leq 2$ when compared to the empirical correlation, and 3) the pitot pressure and Mach number for the Marshall and Kurkov case. A discrepancy of less than 10% is observed on the basis of 1) the skin friction over a flat plate in the range $0 \leq M \leq 6$, 2) the species volume fraction for the Marshall and Kurkov case, 3) the maximum injectant mass fraction for the Waitz et al. case, and 4) injectant mole fraction contours for the Donohue et al. case.

A grid-induced error of less than 2% is observed in the skin-friction coefficient when using a mesh of $392 \times 300$ nodes spanning the flat plate domain. For the shear layer simulations, it was necessary to increase the grid size to $762 \times 320$ nodes to reduce the error on the shear layer growth to less than 6%. The main difficulty in capturing the growth of the shear layer accurately originates from the discontinuity of the turbulent properties at the edges of the shear layer. Another case that is here observed to require a particularly fine mesh is the Settles et al. shock/boundary-layer interaction problem. Even when a mesh composed of $880 \times 440$ nodes is used, an error of 20% is estimated on the streamwise length of the recirculation region. This is postulated to occur for two reasons: 1) a high number of gridlines are needed in the boundary layer due to the very small wall distance of 1 $\mu$m necessary to capture the skin friction and boundary-layer height accurately and 2) a high number of nodes are needed to resolve the viscous profiles inside the thin shock at the point where the shock interacts with the boundary layer. For the mixing problems of Marshall and Kurkov, Waitz et al., and Donohue et al., a relatively modest mesh size is needed to capture the species mass fractions with acceptable accuracy at different streamwise stations. However, it is cautioned that finer meshes would likely be needed to capture accurately the mixing efficiency of such flowfields when the injectant stoichiometric mass fraction is small: The mixing efficiency is strongly dependent on the flow properties on the edges of the mixing layer, which require a large number of grid points to be resolved properly.

The use of the Wilcox dilatational dissipation correction is seen to be necessary in predicting the compressible shear layer growth, at least in the range $0 \leq M_c \leq 2$. Although the dilatational dissipation correction does not significantly alter the ability of the baseline $k$–$\omega$ model to predict the skin friction over a flat plate correctly, it is here tested only up to a freestream Mach number of 6. It remains questionable whether it is beneficial at a higher flow Mach number. For the Settles et al. shock/boundary-layer interaction problem, the use of the dilatational dissipation is seen to be detrimental because it results in a significant overprediction of the size of the separation bubble. Furthermore, better agreement on the basis of the maximum helium mass fraction decay is obtained without the dilatational dissipation for the Waitz et al. ramp injector case. Note that the turbulent Schmidt number is fixed to 1.0 for the Waitz et al. case. A lower value of Schmidt number $Sc_t$ is expected to induce a more rapid decay of the maximum helium mass fraction, and better agreement could then be obtained with the dilatational dissipation rather than without.

The separate effects of the turbulent Schmidt number and the turbulent Prandtl number is investigated for the Marshall and Kurkov inert planar mixing case. Overall better agreement is obtained when setting both $Pr_t$ and $Sc_t$ to 0.5. For the Donohue et al. air–air swept ramp injector problem, the choice of turbulent Schmidt number is observed to be crucial in predicting the injectant mole fraction contours. At a turbulent Schmidt number of 1.0, the maximum injectant mole fraction obtained numerically is as much as three times the one obtained experimentally. At a turbulent Schmidt number of 0.25, the discrepancy is minimal, and good agreement is observed with the experimental data.

A user-specified parameter $k_{\text{div}}$ is introduced in the current implementation of the specific dissipation rate transport equation to improve the robustness of the pseudotime stepping. It is recommended to set $k_{\text{div}}$ to less than 1/10th of the maximum value of $k$ in the turbulent boundary layer for $M \geq 1$ and to less than 1/100th of the maximum value $k$ for $M < 1$. For flow over a flat plate at a freestream Reynolds number of $5 \times 10^6$/m and temperature of 120 K, this is seen to result in a negligible error on the turbulent boundary-layer thickness and skin-friction coefficient. At a Mach number of 2, setting $k_{\text{div}}$ to half the maximum value of $k$ results in a 10% overprediction of the boundary-layer thickness.

## Acknowledgments

This work has been supported by the Natural Sciences and Engineering Research Council and by the BK21 postdoctoral fellowship. Several helpful comments made by In-Seuck Jeung helped improve the quality of the paper and were greatly appreciated.

## References

[1]Sislian, J. P., and Parent, B., "Hypervelocity Fuel/Air Mixing in a Shcramjet Inlet," *Journal of Propulsion and Power* (to be published).

[2]Guoskov, O. V., Kopchenov, V. I., Lomkov, K. E., and Vinogradov, V. A., "Numerical Research of Gaseous Fuel Preinjection in Hypersonic Three-Dimensional Inlet," *Journal of Propulsion and Power*, Vol. 17, No. 6, 2001, pp. 1162–1169.

[3]Livingston, T., Segal, C., Schindler, M., and Vinogradov, V. A., "Penetration and Spreading of Liquid Jets in an External–Internal Compression Inlet," *AIAA Journal*, Vol. 38, No. 6, 2000, pp. 989–994.

[4]Drummond, J. P., "Enhancement of Mixing and Reaction in High-Speed Combustor Flowfields," *Proceedings of the International Colloquium on Advanced Computation and Analysis of Combustion*, ENAS Publisher, Moscow, 1997, pp. 1–14.

[5]Swithenbank, J., Eames, I. W., Chin, S. B., Ewan, B. C. R., Yang, Z., Cao, J., and Zhao, X., "Turbulent Mixing in Supersonic Combustion Systems," *High-Speed Flight Propulsion Systems*, edited by S. N. B. Murthy and E. T. Curran, Vol. 137, Progress in Aeronautics and Astronautics, AIAA, Washington, DC, 1991, Chap. 6, pp. 341–383.

[6]Drummond, J. P., Carpenter, M. H., and Riggins, D. W., "Mixing and Mixing Enhancement in Supersonic Reacting Flowfields," *High-Speed Flight Propulsion Systems*, edited by S. N. B. Murthy and E. T. Curran, Vol. 137, Progress in Aeronautics and Astronautics, AIAA, Washington, DC, 1991, Chap. 7, pp. 383–456.

[7]Waitz, I. A., Marble, F. E., and Zukoski, E. E., "Investigation of a Contoured Wall Injector for Hypervelocity Mixing Augmentation," *AIAA Journal*, Vol. 31, No. 6, 1993, pp. 1014–1021.

[8]Donohue, J. M., McDaniel, J. C., and Haj-Hariri, H., "Experimental and Numerical Study of Swept Ramp Injection into a Supersonic Flowfield," *AIAA Journal*, Vol. 32, No. 9, 1994, pp. 1860–1867.

[9]Fuller, R. P., Wu, P.-K., Nejad, A. A., and Schetz, J. A., "Comparison of Physical and Aerodynamic Ramps as Fuel Injectors in Supersonic Flow," *Journal of Propulsion and Power*, Vol. 14, No. 2, 1998, pp. 135–145.

[10]Parent, B., Sislian, J. P., and Schumacher, J., "Numerical Investigation of the Turbulent Mixing Performance of a Cantilevered Ramp Injector," *AIAA Journal*, Vol. 40, No. 8, 2002, pp. 1559–1566.

[11]Wilcox, D. C., "Dilatation–Dissipation Corrections for Advanced Turbulence Models," *AIAA Journal*, Vol. 30, No. 11, 1992, pp. 2639–2646.

[12]Settles, G. S., Vas, I. E., and Bogdonoff, S. M., "Details of a Shock-Separated Turbulent Boundary Layer at a Compression Corner," *AIAA Journal*, Vol. 14, 1976, pp. 1709–1715.

[13]Brown, G. L., and Roshko, A., "On Density Effects and Large Structure in Turbulent Mixing Layers," *Journal of Fluid Mechanics*, Vol. 64, 1974, pp. 775–781.

[14]Papamoschou, D., and Roshko, A., "The Compressible Turbulent Shear Layer: an Experimental Study," *Journal of Fluid Mechanics*, Vol. 197, 1988, pp. 453–477.

[15]Dimotakis, P. E., "Turbulent Mixing and Combustion," *High-Speed Flight Propulsion Systems*, edited by S. N. B. Murthy and E. T. Curran, Vol. 137, Progress in Aeronautics and Astronautics, AIAA, Washington, DC, 1991, Chap. 5, pp. 265–340.

[16]Wilcox, D. C., "Reassessment of the Scale Determining Equation for Advanced Turbulence Models," *AIAA Journal*, Vol. 26, No. 11, 1988, pp. 1299–1310.

[17]Marshall, C. B., and Kurkov, A. P., "Analytical and Experimental Study of Supersonic Combustion of Hydrogen in a Vitiated Air Stream," NASA TM X 2828, Sept. 1973.

[18]Drummond, J. P., Rogers, R. C., and Hussaini, M. Y., "Detailed Numerical Model of a Supersonic Reacting Mixing Layer," AIAA Paper 86-1427, June 1986.

[19]Carpenter, M. H., "Three-Dimensional Computations of Cross-Flow Injection and Combustion in a Supersonic Flow," AIAA Paper 89-1870, June 1989.

[20]Lee, S.-H., Jeung, I.-S., and Yoon, Y., "Computational Investigation of Shock-Enhanced Mixing and Combustion," *AIAA Journal*, Vol. 35, No. 12, 1997, pp. 1813–1820.

[21]Parent, B., and Sislian, J. P., "The Use of Domain Decomposition in Accelerating the Convergence of Quasihyperbolic Systems," *Journal of Computational Physics*, Vol. 179, No. 1, 2002, pp. 140–169.

[22]Jachimowsky, C. J., "An Analytical Study of the Hydrogen–Air Reaction Mechanism With Application To Scramjet Combustion," NASA TP 2791, Dec. 1988.

[23]Viviand, H., "Conservative Forms of Gas Dynamics Equations," *La Recherche Aùerospatiale*, No. 1, Jan. 1974, pp. 65–68.

[24]Vinokur, M., "Conservative Equations of Gas-Dynamics in Curvilinear Coordinate Systems," *Journal of Computational Physics*, Vol. 14, 1974, pp. 105–125.

[25]Yee, H. C., Klopfer, G. H., and Montagné, J.-L., "High-Resolution Shock-Capturing Schemes for Inviscid and Viscous Hypersonic Flows," *Journal of Computational Physics*, Vol. 88, 1990, pp. 31–61.

[26]Laney, C. B., *Computational Gasdynamics*, Cambridge Univ. Press, Cambridge, England, U.K., 1998.

[27]McBride, B. J., and Reno, M. A., "Coefficients for Calculating Thermodynamic and Transport Properties of Individual Species," NASA TM 4513, Oct. 1993.

[28]Briley, W. R., and McDonald, H., "Solution of the Multidimensional Compressible Navier–Stokes Equations by a Generalized Implicit Method," *Journal of Computational Physics*, Vol. 24, 1977, pp. 372–397.

[29]Beam, R., and Warming, R. F., "An Implicit Factored Scheme for the Compressible Navier–Stokes Equations," *AIAA Journal*, Vol. 16, No. 4, 1978, pp. 393–402.

[30]Wilcox, D. C., *Turbulence Modeling for CFD*, DCW Industries, La Cañada, CA, 1994.

[31]Sarkar, S., Erlebacher, G., Hussaini, M. Y., and Kreiss, H. O., "The Analysis and Modeling of Dilatational Terms in Compressible Turbulence," *Journal of Fluid Mechanics*, Vol. 227, June 1991, pp. 473–493.

[32]Brown, G. L., "The Entrainment and Large Structure in Turbulent Mixing Layers," *Proceedings of the 5th Australasian Conference on Hydraulics and Fluid Mechanics*, Christchurch, New Zealand, 1974, pp. 352–359.

[33]Parent, B., and Sislian, J. P., "Effect of Geometrical Parameters on the Mixing Performance of Cantilevered Ramp Injectors," *AIAA Journal*, Vol. 41, No. 3, 2003, pp. 448–456.

R. So
*Associate Editor*